Samson Galvin
Mechanical Engineering,
Department of Mechanical Engineering,
The Pennsylvania State University,
University Park, PA 16802
e-mail: sfg5341@psu.edu

Rachael Kate Yanalitis
Mechanical Engineering,
Department of Mechanical Engineering,
The Pennsylvania State University,
University Park, PA 16802

Eric Leon
Mechanical Engineering and
Biomedical Engineering,
Department of Mechanical Engineering,
The Pennsylvania State University,
University Park, PA 16802

Joshua Winder
Hershey Medical Center,
Hershey, PA 17033

Randy Haluck
Professor
Hershey Medical Center,
Hershey, PA 17033

Paris von Lockette
Professor
Mechanical Engineering,
Department of Mechanical Engineering,
The Pennsylvania State University,
University Park, PA 16802

Jason Z. Moore[1]
Professor
Mechanical Engineering,
Department of Mechanical Engineering,
The Pennsylvania State University,
University Park, PA 16802
e-mail: jzm14@psu.edu

Design of the Novel Single Incision, Free Motion Laparoscopic Surgical System

Laparoscopic surgery is a common minimally invasive surgery that uses specialized tools to access the abdominal cavity and pelvic regions via small incisions called ports. Compared to open surgery, laparoscopy's small incision size better protects a patient's health and reduces recovery time. However, restricted rotation of the tools around chosen port locations can limit a surgeon's mobility while operating. To address this, the novel single incision, free motion (SIFM) laparoscopic surgical system was created, and its design was explored through three experiments. Experiment 1 analyzed different permanent magnetic configurations to optimize the magnetic force between a tool on the inside of the abdominal wall and an external tool. The chosen configuration was a single-pole external magnet, coupled to an axially magnetized internal magnet. Experiment 2 analyzed the experimental and theoretical forces applied by the internal tool. The tool was able to provide sufficient cutting forces at 26.1 mm of separation between the tools. Experiment 3 measured the precision of the tool's end effector which was controlled by a stepper motor-powered cable system. The tool's end effector rotates no more than 1 deg about the y*-axis and no more than 2 deg about the* x*-axis. The SIFM system combines the health benefits of minimally invasive laparoscopic surgery, with the free motion and ease of open surgery.*
[DOI: 10.1115/1.4062178]

Keywords: laparoscopic surgery, minimally invasive, permanent magnet, cable system

Introduction

Laparoscopic surgery offers numerous advantages over traditional open surgery. The smaller incisions used in laparoscopic procedures reduce scarring, surgical site infections, patient pain, and decrease recovery time [1,2]. These significant advantages are due to the smaller incision size used in laparoscopic procedures. As compared to the 10 cm incision along the abdomen used in open surgery [3], laparoscopic surgery needs approximately three to five 1–2 cm keyhole incisions around the abdomen, while pressurized CO_2 gas expands the abdominal cavity [4]. Since the first laparoscopic procedure was performed in 1987, interest in minimally invasive procedures continues to increase [5], and currently, nearly 15×10^6 laparoscopic surgeries occur annually around the world [6].

Although laparoscopic surgery has many health benefits for the patient, surgeons can experience several drawbacks while using this procedure. To perform laparoscopic procedures, additional training is required, and the limited movement can lengthen the time of the procedure. Traditional laparoscopic surgery requires fixed port locations, specialized tools, and instruments that can only pivot around the selected incisions. These limiting factors may require surgeons to add additional ports or lengthen pre-existing ports. Port size is one of the main risk factors in trocar site hernias [7]. Adding additional ports will increase recovery time and increase the risk of hernias which occur in 1.5%–1.8% of all laparoscopic procedures [7]. Compensation for the tool's limited motion around the trocar locations reduces laparoscopic surgery's benefits. The decrease in mobility and control also increases the surgery time. One study reports an average of 30 min more time was required for a laparoscopic colectomy compared to open surgery for the same operation [1]. Additionally, surgeons require longer training time to develop proficiency. One study showed that 200–250 patient cases are needed to gain full proficiency in laparoscopic prostatectomy [2].

With the novel SIFM laparoscopic tool design, surgeons control the tools through the skin in an active fashion. Figure 1 illustrates the tool's magnetic connection through an abdominal wall. The operating surgeon controls the external tool and can move freely around the outside of the abdominal wall with an adjustable force between components. The internal tool can slide into the abdominal cavity via a port near the umbilicus. A cable system is fed through the port and controls the internal tool's end effector. A Teflon casing

[1]Corresponding author.
Manuscript received September 12, 2022; final manuscript received March 2, 2023; published online April 19, 2023. Assoc. Editor: Med Amine Laribi.

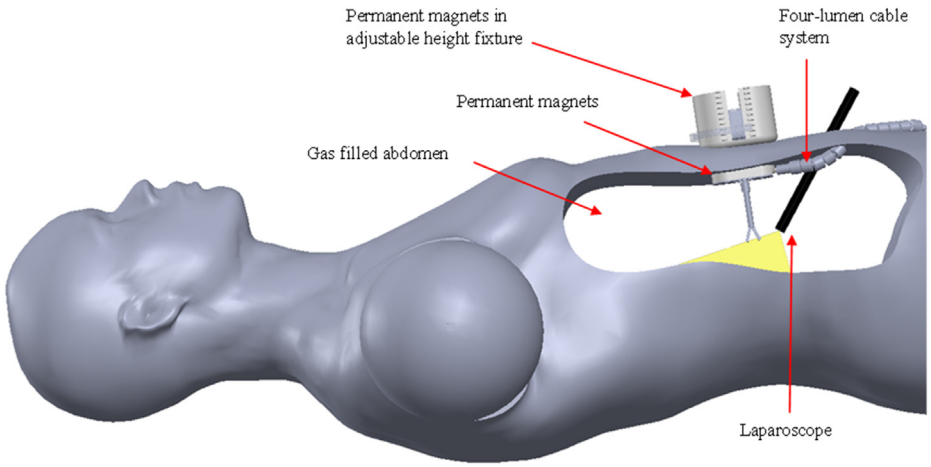

Fig. 1 Novel single incision, free motion (SIFM) laparoscopic surgical system

around both tools reduces the coefficient of friction when sliding across the skin. The SIFM laparoscopic system, introduced in this paper reduces the number of ports needed for a single incision and enables free motion inside the abdominal wall.

Currently, there is a lot of research in the field of remote operations of laparoscopic tools. Robot-assisted surgery increases precision and improves proficiency [9,10]. Furthermore, several studies on hand recognition for surgical robot control have been conducted to further improve human-robot interaction [11,12]. Robot-assisted surgery and the operator's hand motion and control will ultimately affect the precision of the SIFM device, and fortunately, there is a lot of work being done in this area.

Several studies have explored the use of magnets to aid surgical procedures [13–17]. In previous studies, capsular endoscopes and magnetic endoscopes have been controlled externally via a magnetic connection [14,15]. The SIFM device is uniquely able to manipulate tissue with larger forces and to account for larger expected forces during laparoscopic surgery compared to a colonoscopy. The internal tool's body was controlled similarly to the capsular endoscopes and magnetic endoscopes but had additional degrees-of-freedom. The SIFM tool had six degrees-of-freedom: translation and rotation on the surface of the abdominal cavity due to the magnetic connection, two additional rotations due to the cable system, and height translation from pushing or pulling on the inflated abdominal cavity.

Levita magnetics developed a purely stationary internal magnetic clip that uses permanent magnets to retract tissue away from the working area, which the FDA approved in 2016 [13,17]. The design is made to hold tissue stationary and not actively manipulate it during surgery. The SIFM design allows for operational control of surgical tools to cut, grasp, and lift the tissue. Additionally, multiple ports are still required with the use of a magnetic clip. Furthermore, a similar approach proposed by Florence Leong uses a magnetic surgical instrument to control a tool on the inside of the abdominal cavity and its end effector, published in January 2016 [16]. This design uses magnetic coupling to control the end effector. The model, with only four degrees-of-freedom, has difficulty repositioning due to its body size of 12.7 mm in diameter and 120 mm in length. The SIFM design has a smaller overall size and six degrees-of-freedom due to the tendon-driven spring joint. The end effector is controlled with a cable system that uses a lumen body backbone. The base of the end effector moved independently of the cable system and the tendon-driven cable system controls the end effector when the tool is in the desired position. Furthermore, the SIFM tool design uses similar cable systems to recent research initiatives. A team from State Key Laboratories analyzed a pully cable system for the gripper of a laparoscopic robot in 2017 [18]. And current endoscope designs use similar cable control systems [19,20]. The SIFM laparoscopic system accurately controls the tool's end effector with a cable system based on similar research but is capable of changing the base location with an external magnetic connection. In the scope of this paper, we address the accuracy of the motor-controlled tendon-driven end effector and the strength of the magnetic forces. Understanding the accuracy of this system is important for the later development of the controls of the system.

This paper introduces the novel SIFM laparoscopic surgical system and evaluates its performance. In this paper, the materials and methods used to create the SIFM prototype are presented, as well as the materials and methods to create the three experiments that evaluate SIFM performance. Results are then presented followed by conclusions.

Materials and Method

Three different experiments generated data on the SIFM laparoscopic tool. Experiment 1 focused on optimizing the magnetic attractive force between the external and internal tools using ANSYS (Canonsburg, PA) simulation software. Experiment 2 analyzed the maximum applied forces and torques of the internal tool via the magnetic connection. Experiment 3 measured the precision of the cable system used to control the internal tool's end effector.

In experiment 1, six magnetic permutations were analyzed using ANSYS simulation software and were variations of single pole magnets and dual pole magnets across three subcategories: axial, radial, and permeable disk. Because the single and dual pole magnets are outside of the body, they did not share the same limitations as the internal magnets. The simulations modeled the single pole magnets as two axially magnetized neodymium magnets with one north pole upward and the other south pole upward. The dual pole magnets were the same size as the single pole but were modeled as a magnetic disk inside a magnetic ring, with the ring's north pole upward, and the center disk with its south pole upward. To have easily comparable data, the sizes of each magnet and spacing apart remained the same in each permutation. The axial magnets are grade N-52 (residual induction of ~14.5 mT), the radial magnets are grade N-50 (residual induction of ~14.2 mT), and the permeable disk is modeled as cobalt-iron (relative permeability of 18,000). The axial magnets are from K&J Magnetics (Jamison, PA), and the radial magnets are from SuperMagnetMan (Pelham, AL).

Both experiments 2 and 3 utilized the SIFM device designed and fabricated as shown in Fig. 2. The SIFM device regulates the magnetic force with adjustable separation of the internal and external magnets. The surgeon can adjust the external tool's height to account for muscle, fat, and tissue thickness changes while moving around the abdominal wall. The external system relies on feedback from two force sensing resistors (Pololu, Las Vegas, NV) that measure the attractive force between the internal and external magnets and can be adjusted on ranges from 0 mm to 38.1 mm. A set

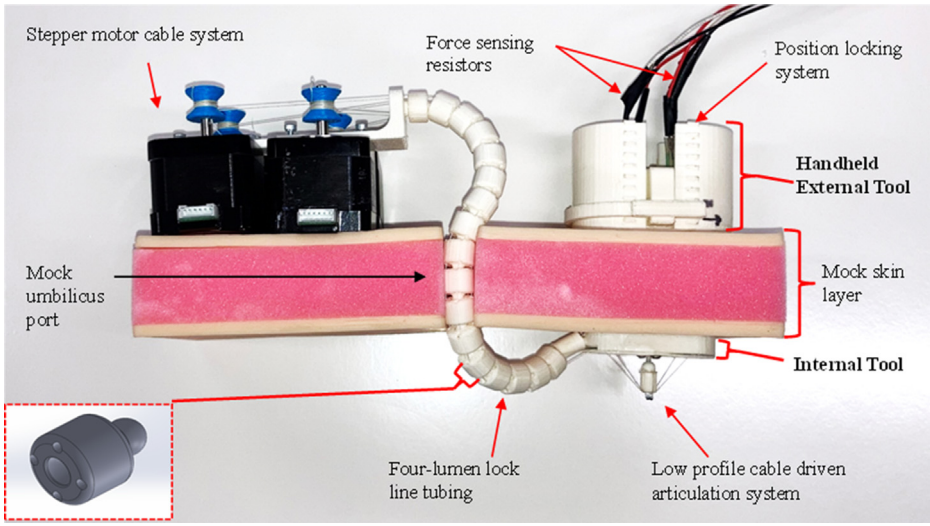

Fig. 2 SIFM internal and external tools

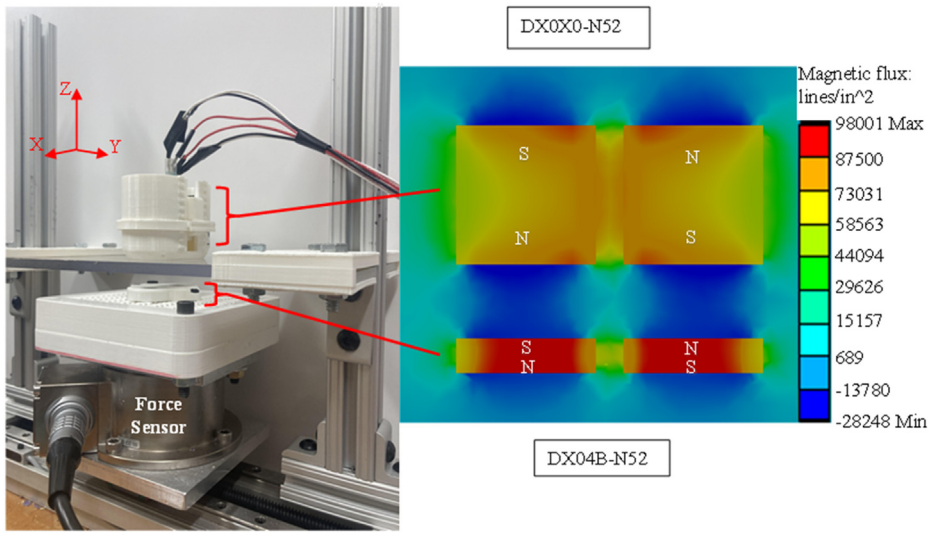

Fig. 3 Experimental setup to measure magnetic forces and torques in the *x*-, *y*-, and *z*-directions

of two oppositely poled axial magnets are used in both tools. The magnets selected were grade N-52 neodymium magnets from K&J Magnetics. When inserted into the body, the tool will lay horizontally to reduce the overall profile [21]. The insertion profile is 29 mm wide and 10 mm tall, in addition to the area of the surgical tool attached to the end effector. The part is 59.5 mm in length. Rigid PLA plastic encased each set of magnets, and the base is wrapped in Teflon to reduce friction when sliding across skin and tissue. The extensive testing that evaluated low-friction materials sliding over porcine skin determined Teflon as the desired material as reported by Galvin [22]. Additional control of the tool's end effector is provided through a motor-driven cable system. A spring joint attached the cable system and the tool to the magnetic base. Four-lumen lock line tubes created the tubing system that housed these cables.

Experiment 2 measured the maximum forces and torques of the magnetic system at different distances apart utilizing the SIFM device along with the experimental setup shown in Fig. 3. Magnetic position was varied in the *x*- and *y*-plane, and rotation about the *z*-axis, while the force was collected using the ATI gamma IP65 force sensor (ATI Industrial Automation, Apex, NC). Data collected in experiment 2 were compared to calculated data from ANSYS simulations. Both ANSYS and sensor testing measured the forces and torques provided by the magnetic connection at separation distances from 9.5 mm to 38.1 mm, with 3.2-mm increments.

The maximum force in the *z*-direction occurs when the internal and external magnets are concentric, as shown in the image on the right in Fig. 3. The maximum force in the *x*- and *y*-directions is found when the external tool is shifted along its respective axis. However, the shift along an axis reduces the force in the *z*-direction. Therefore, at the maximum *x*- and *y*-forces, the maximum *z*-force is recorded as well. The maximum torque was found by rotating the external tool around the *z*-axis, again this rotation decreases the maximum *z*-force. Testing recorded six forces and one torque at each separation distance. Experimental force results were compared to ANSYS simulation results.

Experiment 3 measured the precision of the internal tool's end effector, controlled by a cable system and stepper motors. MATLAB (MathWorks, Natick, MA) analyzed the angle of the tool's end effector as it rotated about the *x*- and *y*-axis. The rotation about the *x*- and *y*-axis occurred independently of one another to keep the calculations simple. A video recorded the tool's end effector rotating from approximately 180 deg (horizontal) to 0 deg, then back up to 90 deg (vertical). Figure 4 displays the three individual frames of the

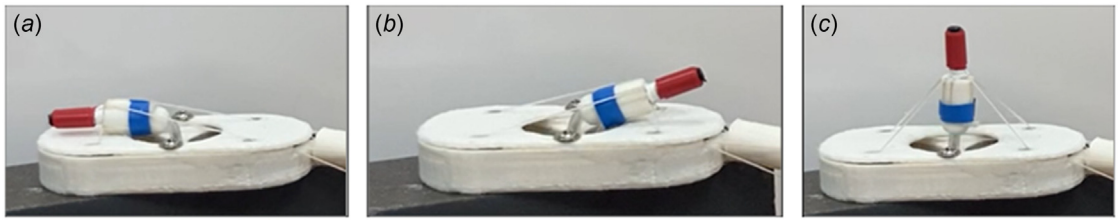

Fig. 4 Image of starting position (*a*) (∼180 deg) maximum rotation angle (*b*) (∼20 deg) and ending vertical position (*c*) (90 deg) recorded for MATLAB analysis

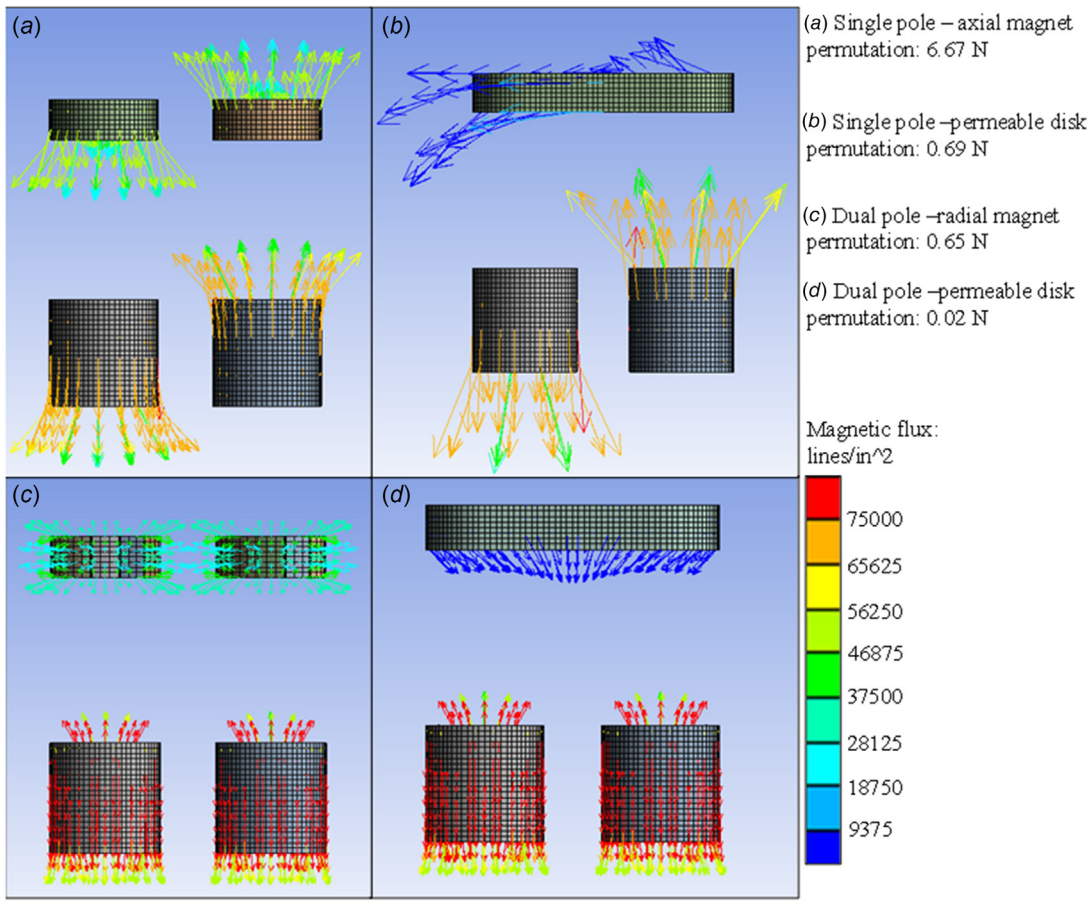

Fig. 5 ANSYS magnetic flux and force simulation results for four of the six magnet permutations

video MATLAB used to analyze the tool angle. The tool's tip and base are marked with different bands. The centroid locations of the bands were found in MATLAB and used to calculate the tool's angle. Data were collected on rotation about the *y*-axis (images shown in Fig. 4) and the *x*-axis.

Results and Discussion

The results from experiment 1 created the design of the internal and external tools that experiments 2 and 3 analyzed. Experiment 1 optimized the magnetic configuration of the internal and external tools with the use of ANSYS's computer modeling software. Figure 5 displays the magnetic flux densities and resulting forces from experiment 1. The figure only contains four out of the six considered permutations and excluded the single pole external magnet—radial internal magnet and dual pole—axial internal magnet configurations because their net force approached 0 N. In both excluded permutations, the magnetic configurations created counteractive magnetic fields, resulting in a net attractive force of less than 0.001 N.

The single pole configuration, shown in Figs. 5(*a*) and 5(*b*), provided higher forces at a separation distance of 38.1 mm than the dual pole configuration. For the magnet sizes chosen in this experiment, the single-pole magnets were stronger at farther distances, and dual-pole magnets were stronger at closer distances. Because muscle, fat, and tissue separate the internal and external tools during surgery, the SIFM design requires a magnetic configuration that is stronger at farther distances. The configuration with the highest force was the single pole–axial magnet configuration which produced 6.67 N. The single pole–permeable disk produced the second most force of 0.69 N. In future designs, a combination of the permeable disk and the axial internal magnet will produce additional magnetic forces. Furthermore, a magnetic yoke or strong electromagnets could become a potential alternative instead of an external permanent single-pole axial magnet. With a magnetic yoke, the field easily adjusts with a change in current, instead of the current system that relies on adjusting the magnet's height to control forces between the internal and external magnets. One method to increase the holding force of the single pole–axial configuration would be to make both sets of magnets similarly poled,

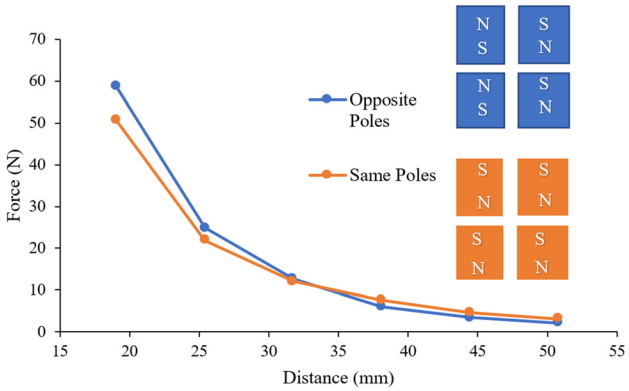

Fig. 6 Experimentation force results for two different configurations of four magnets

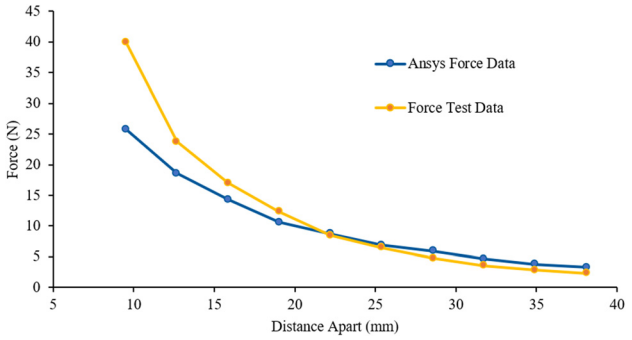

Fig. 7 ANSYS calculated data and experimental data comparison

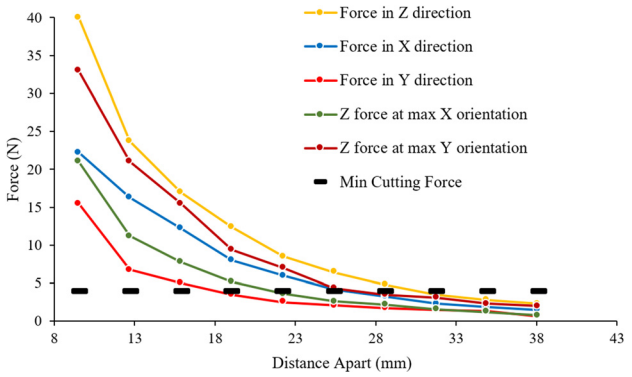

Fig. 8 Experimentation results for maximum forces in the *x*-, *y*-, and *z*-directions of the internal tool

and both the magnet's north poles would face downward. Figure 6 provides a forced comparison between two tests where the magnets were similarly poled, and another set oppositely poled. Although the opposite poled design creates weaker forces at farther distances, it provides a far stronger torque compared to similar poled magnets. When both poles are the same, there is no repelling force when the external magnet rotates, resulting in very weak torques on the internal magnet. The chosen internal magnets minimized the magnets sizing while obtaining the necessary forces needed for surgery.

Experiment 2 tested the three forces and torques for the single pole-axial magnetic configuration and was compared to calculated results from the ANSYS simulations. Table 1 presents the data for experiment 2 and Fig. 7 illustrates the values for the maximum pulling force for both ANSYS simulation and experimental data. There is a minimal error in the calculated data versus experimental data after around 19 mm. However, the error in the first four data points can be accounted for by the chosen meshing size of the calculated data and the chosen residual flux density. For a grade N-52 neodymium magnet, the typical residual flux density is between 1430 and 1480 mT. Additional errors arose when purchasing magnets because there is no standard practice for measuring the grade of a magnet. In this case, we can assume the residual flux density resides in the upper range because the experimental data collected was higher than the calculated data. A more refined mesh would decrease the error in the dataset as well but increases simulation time considerably.

The force decreases exponentially as the distance between internal and external magnets increases from 9.5 mm to 38.1 mm, resulting in forces of 40 N down to 2.22 N, respectively. The maximum forces in the *x*- and *y*-directions as well as torque decrease at an exponential rate similar to the decrease in force in the *z*-direction. Figure 8 visualized the relationships between maximum forces at each separated distance. Testing showed that the applied force in the x direction is around twice the force applied in the y direction for all distances. However, the attractive force when the maximum force is applied in the *x*-direction is about half the attractive force when the maximum force is applied in the *y*-direction. The magnetic configuration caused this difference in *x*- and *y*-directional forces. A shift in the *x*-axis causes an additional repelling force from the internal magnet with the north pole facing upward, and the external magnet with the north facing downward. As the north pole of the external magnet started to shift over the north pole of the internal magnet, there is more force provided in the *x*-direction and less holding force because of the resultant repulsive force.

In practice, layers of muscle, fat, and skin tissue would separate the magnets. Depending on the location of the magnet in the abdomen, the rectus abdominus, or internal and external obliques, and the transverse abdominis would separate the internal and external tools. On average the rectus abdominus and transverse abdominal muscle are approximately 14.9 mm thick in men, and

Table 1 Forces and torques of the magnetic system from 9.5 mm to 38.1 mm

Separation distances (mm)	Maximum force in *X* (N)	Maximum force in *Y* (N)	Maximum force in *Z* (N)	*Z* force at maximum *X*-orientation (N)	*Z* force at maximum *Y*-orientation (N)	Torque about *Z*-axis (N-m)	*Z* force at maximum torque (N)	ANSYS maximum *Z*-force (N)
9.5	22.25	15.50	40.00	21.00	33.00	0.38	38.75	25.81
12.7	16.25	6.75	23.75	11.25	21.00	0.31	17.35	18.63
15.9	12.25	5.00	17.00	7.75	15.50	0.25	12.00	14.27
19.1	8.00	3.50	12.35	5.15	9.40	0.20	5.85	10.58
22.2	6.00	2.50	8.50	3.60	7.00	0.14	5.30	8.70
25.4	4.20	2.10	6.42	2.60	4.30	0.09	4.00	6.92
28.6	3.25	1.75	4.75	2.20	3.50	0.07	3.35	5.92
31.8	2.30	1.50	3.50	1.60	3.10	0.05	2.20	4.62
34.9	1.85	1.30	2.80	1.20	2.35	0.04	2.00	3.78
38.1	1.50	0.60	2.30	0.80	2.00	0.03	1.80	3.29

Fig. 9 MATLAB video analysis of tool movement about the *y*-axis

12.2 mm thick in women [23]. The average transverse abdominis and external and internal oblique thickness are approximately 19.1 mm in men and 14.4 mm in women [23]. There is limited data on fat thickness because it varies drastically based on the patient and is highly compressible [24]. However, skin and subcutaneous tissue thickness can range from 2.2 to 28.1 mm in males and 5.2–27.4 mm in females [25]. For the full range of motion in the abdominal wall, the laparoscopic tool would function effectively on patients with a skin and subcutaneous tissue thickness of less than approximately 7 mm in males and 11.7 mm in females. At this skin and tissue thickness, the internal and external tools are separated by a maximum distance of 26.1 mm. As shown in Fig. 8, the maximum force applied in the x direction is 4 N at 26.1 mm, which is equal to the force required to cut into porcine ascending aorta tissue [26]. And the force required to cut into porcine tissue is comparable to human tissue aged under 60 [27,28]. When the force in the x direction is maximized at 26.1 mm, the holding force is 2.02 N. When no force is applied in the x or y direction, the maximum holding force increases to 6.05 N. Therefore, the expected holding force when cutting at the maximum separation distance assumedly resides between 2.02 N and 6.05 N. To summarize, the SIFM external tool can provide a sufficient cutting force on ascending aorta tissue, while maintaining between 2.02 N and 6.05 N of holding force.

Experiment 3 tested the precision of the stepper motor cable system. The internal tool was connected to the stepper motors on the outside of the body via a four-lumen lock line tubing system. During tool control, the tube can bend freely. As the tube bends, one cable will become slacker, and the cable on the other side of the tube will be taut. A four-lumen tube is crucial to keep the cables separated, otherwise, the overlapping of the cables would prevent the tool from moving. Furthermore, a lock line system allows bending while keeping the material rigid. If the cables were housed by a rubberlike tubing system, there would be higher friction between the cables and the rubber interior wall. The resulting high friction would stop the movement of the cables and thus the end effector. A more flexible tube allows for easier deflection of the internal system instead of pulling the cable through the tube and moving the end effector. This experiment used four Nema 17 stepper motors (STEPPERONLINE, New York), each with a maximum torque of 45 N-cm. The internal tool is controlled with four cables, each attached to an individual stepper motor. The cables are wired independently of each other to allow for slack and tension control. Each step from the stepper motor changes the angle of the end effector slightly by changing the triangle side a shown in Fig. 9(*a*). The angle (A) is calculated with the law of cosines equation

$$A = (\cos^{-1}(b^2 + c^2 - a^2)) * \frac{1}{2 * b * c} \tag{1}$$

where a, b, and c are sides of the triangle formed by the cable, base, and tool, respectively. The calculated data can be compared to the actual tool effector angle which is measured using MATLAB. The centroid of the red and blue color bands is shown in Fig. 9(*b*). From the centroid locations, the actual angle is calculated as the tool rotates from 180 deg (horizontal) to 0 deg, then back to 90 deg. Figure 9 presents the tool at 90 deg rotating about the *y*-axis.

At each frame of the video, MATLAB records the pixel locations of the bands to gather experimental position data on the tool angle. Figure 10 illustrates the calculated tool angle using Eq. (1) and the actual angle as the tool rotates around the *y*-axis. The calculated plot shares a similar shape to the experimental plot but shifts to the right. This shift indicates a delay in the experimental tool's response time to the stepper motors changing the cable length.

After the 8-second mark and before the 70-second mark, the calculated plot predicts a quicker angle adjustment as presented in Fig. 10. This relationship is shown by the calculated data being several degrees lower than the experimental data and a steeper slope on the calculated tool angle. The stepper motors picking up the slack in the cable caused the initial delay in the experimental data. The longer the cable and tube system, the more delay can be expected between direction changes of the tool. Other sensors can be added to reduce the possible error that can occur from this delay. During rotation about the *y*-axis, each step from the stepper motor is 1 deg at maximum, and when the tool adjusts for slack, each step will move the tool less than 1 deg. At 80 s in Fig. 10, the tool reaches the end of its rotation and starts moving back upward to 90 deg. After the 80-second point, the delay in rotation occurs again as the experimental data takes more time to move compared to the calculated data. Figure 11 illustrates the tool response for the rotation of the *x*-axis. Because the cable port locations are placed closer to the base of the end effector, the rotation about the *x*-axis is less precise than the rotation about the *y*-axis.

Each step from the motor results in about two degrees of motion in the tool's angle. For rotation about the *y*-axis, rotations require about 80 s, compared to the 40 s spent rotating about the *x*-axis. The

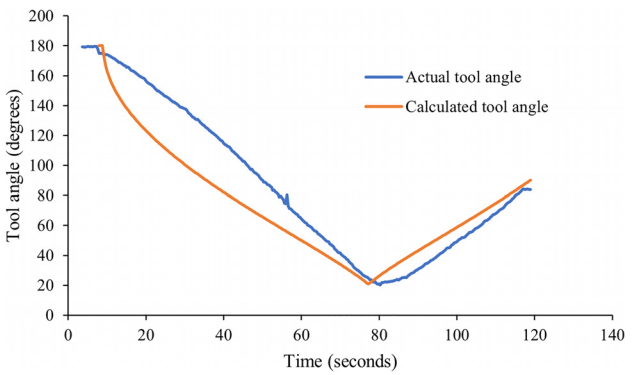

Fig. 10 Experimental and calculated data for the end effector rotating about the internal tool's *y*-axis

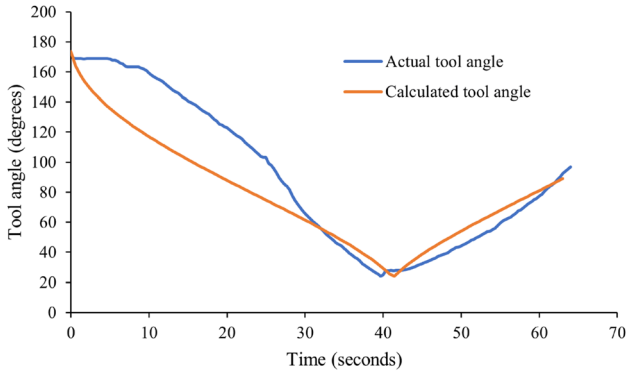

Fig. 11 Experimental and calculated data for the end effector rotating about the internal tool's *x*-axis

y-rotation plot, as seen in Fig. 11, displays the same delay relationship as the rotation delay about the *x*-axis. The results supported that a step will be less than a degree of rotation of the tool when rotating about the *y*-axis. Similarly, a step about the *x*-axis will result in less than 2 deg in rotation of the tool. During large movements, the law of cosines Eq. (1), can model the shape of the tool's rotation with the cable length as the dependent variable. If the tool rotates about multiple axes, the tool's height would become another dependent variable. Furthermore, the movement of the lock line system can affect the angle of the end effector. When the internal part is stationary, the movement of the lock line system will cause the end effector to move less with each step due to the backbone structure's shape being modified. In future use, the position of the end effector will be recorded with the laparoscope and the effects from the modified backbone will be accounted for by overstepping until the end effector is in position. In future designs, the end effector will be locked in position if the internal tool base is in motion to stop any unwanted end effector changes from the backbone changing shape.

Conclusion

The novel single incision, free motion (SIFM) laparoscopic surgical system used an optimized magnetic configuration to minimize the internal tool's profile while maintaining a strong magnetic connection through the skin. The second experiment analyzed the resulting forces and torques of the planar joint created by the magnetic connection to determine the maximum skin and subcutaneous tissue thickness where the SIFM tool could sustain strong enough attractive forces. The external tool provides feedback on the forces between the magnets and the height can be adjusted to optimize the magnetic connection. The internal tool can apply the necessary forces required in laparoscopic surgery when the overall distance between the internal and external tools is less than or equal to 26.1 mm. The third experiment analyzed the precision of the tool's end effector controlled by the cable system. With stepper motor control provided outside of the body, the end effector will rotate no more than 1 deg about the *x*-axis and no more than 2 deg about the *y*-axis for each motor step. Future research will explore new magnetic configurations to find stronger forces and more controllable magnetic connections. Moreover, future testing will evaluate new tubing and cable systems to further improve the accuracy of the internal tool's end effector.

Funding Data

- The Pennsylvania State University Center for Biodevices (Biodevices Seed Grant; Funder ID: 10.13039/100008321).

Data Availability Statement

The datasets generated and supporting the findings of this article are obtainable from the corresponding author upon reasonable request.

References

[1] Veldkamp, R., Kuhry, E., Hop, W. C., Jeekel, J., Kazemier, G., Bonjer, H. J., Haglind, E., et al., 2005, "Laparoscopic Surgery Versus Open Surgery for Colon Cancer: Short-Term Outcomes of a Randomised Trial," Lancet Oncol., **6**(7), pp. 477–484.

[2] Secin, F. P., Savage, C., Abbou, C., de La Taille, A., Salomon, L., Rassweiler, J., Hruza, M., et al., 2010, "The Learning Curve for Laparoscopic Radical Prostatectomy: An International Multicenter Study," J. Urol., **184**(6), pp. 2291–2296.

[3] McMillan, A., 2021, "Minimally Invasive Surgery vs. Open Surgery: What's the Difference?," Evansville Surgical Associates, Evansville, IN, accessed Jan. 13, 2022, https://www.evansvillesurgical.com/minimally-invasive-surgery-vs-open-surgery-whats-the-difference/

[4] Tsai, F. S., Johnson, D., Francis, C. S., Cho, S. H., Qiao, W., Arianpour, A., Mintz, Y., Horgan, S., Talamini, M., and Lo, Y. H., 2010, "Fluidic Lens Laparoscopic Zoom Camera for Minimally Invasive Surgery," J. Biomed. Opt.. **15**(3), p. 030504.

[5] Vecchio, R., MacFayden, B. V., and Palazzo, F., 2000, "History of Laparoscopic Surgery," Panminerva Med., **42**(1), pp. 87–90.

[6] Wood, L., 2018, "Global Laparoscopy and Endoscopy Devices Market, 2025 - Focus on Surgical Procedures (Cholecystectomy and Hysterectomy) and Product Types (Arthroscopes, Neuroendoscopes, Cystoscope, and Bronchoscopes)," Research and Markets, https://www.globenewswire.com/news-release/2018/09/19/1572863/0/en/Global-Laparoscopy-and-Endoscopy-Devices-Market-2025-Focus-on-Surgical-Procedures-Cholecystectomy-and-Hysterectomy-and-Product-Types-Arthroscopes-Neuroendoscopes-Cystoscope-and-Bro.html

[7] Wells, A., Germanos, G. J., Salemi, J. L., and Mikhail, E., 2019, "Laparoscopic Surgeons' Perspectives on Risk Factors for and Prophylaxis of Trocar Site Hernias: A Multispecialty National Survey," JSLS, **23**(2), p. e2019.00013.

[8] Berguer, R., Smith, W. D., and Chung, Y. H., 2001, "Performing Laparoscopic Surgery is Significantly More Stressful for the Surgeon Than Open Surgery," Surg. Endosc., **15**(10), pp. 1204–1207.

[9] Su, H., Qi, W., Chen, J., and Zhang, D., 2022, "Fuzzy Approximation-Based Task-Space Control of Robot Manipulators With Remote Center of Motion Constraint," IEEE Trans. Fuzzy Syst., **30**(6), pp. 1564–1573.

[10] Su, H., Mariani, A., Ovur, S. E., Menciassi, A., Ferrigno, G., and De Momi, E., 2021, "Toward Teaching by Demonstration for Robot-Assisted Minimally Invasive Surgery," IEEE Trans. Autom. Sci. Eng., **18**(2), pp. 484–494.

[11] Ovur, S. E., Su, H., Qi, W., De Momi, E., and Ferrigno, G., 2021, "Novel Adaptive Sensor Fusion Methodology for Hand Pose Estimation With Multileap Motion," IEEE Trans. Instrum. Meas., **70**, pp. 1–8.

[12] Qi, W., Ovur, S. E., Li, Z., Marzullo, A., and Song, R., July 2021, "Multi-Sensor Guided Hand Gesture Recognition for a Teleoperated Robot Using a Recurrent Neural Network," IEEE Rob. Autom. Lett., **6**(3), pp. 6039–6045.

[13] Levita Magnetics, 2018, "Levita Magnetics Announces FDA Clearance of Expanded Indication for Magnetic Surgical System for Use of Bariatric Procedures," Levita Magnetics Announces FDA Clearance of Expanded Indication for Magnetic Surgical System for Use in Bariatric Procedures | Business Wire, accessed Mar. 28, 2023, https://www.businesswire.com/news/home/20181022005267/en/Levita%C2%AE-Magnetics-Announces-FDA-Clearance-of-Expanded-Indication-for-Magnetic-Surgical-System-for-Use-in-Bariatric-Procedures

[14] Ciuti, G., Valdastri, P., Menciassi, A., and Dario, P., 2010, "Robotic Magnetic Steering and Locomotion of Capsule Endoscope for Diagnostic and Surgical Endoluminal Procedures," Robotica, **28**(2), pp. 199–207.

[15] Martin, J. W., Scaglioni, B., Norton, J. C., Subramanian, V., Arezzo, A., Obstein, K. L., and Valdastri, P., 2020, "Enabling the Future of Colonoscopy With Intelligent and Autonomous Magnetic Manipulation," Nat. Mach. Intell., **2**(10), pp. 595–606.

[16] Leong, F., Garbin, N., Di Natali, C., Mohammadi, A., Thiruchelvam, D., Oetomo, D., and Valdastri, P., 2016, "Magnetic Surgical Instruments for Robotic Abdominal Surgery," IEEE Rev. Biomed. Eng., **9**, pp. 66–78.

[17] Rivas, H., Robles, I., Riquelme, F., Vivanco, M., Jiménez, J., Marinkovic, B., and Uribe, M., 2018, "Magnetic Surgery: Results From First Prospective Clinical Trial in 50 Patients," Ann. Surg., **267**(1), pp. 88–93.

[18] Renfeng, X., Bingyin, R., Zhiyuan, Y., and Zhijiang, D., 2017, "A Cable-Pulley System Modeling Based Position Compensation Control for a Laparoscope Surgical Robot," Mech. Mach. Theory, **118**, pp. 283–299.

[19] Burgner-Kahrs, J., Rucker, D. C., and Choset, H., 2015, "Continuum Robots for Medical Applications: A Survey," IEEE Trans. Rob., **31**(6), pp. 1261–1280.

[20] Dupont, P. E., Simaan, N., Choset, H., and Rucker, C., 2022, "Continuum Robots for Medical Interventions," Proc. IEEE, **110**(7), pp. 847–870.

[21] Yamanaka, H., Makiyama, K., Osaka, K., Nagasaka, M., Ogata, M., Yamada, T., and Kubota, Y., 2015, "Measurement of the Physical Properties During Laparoscopic Surgery Performed on Pigs by Using Forceps With Pressure Sensors," Adv. Urol., **2015**, pp. 1–10.

[22] Galvin, S., Yanalitis, R., Winder, J., Haluck, R., von Lockette, P., and Moore, J., 2022, "Selection of Low Friction Material for Novel Single Incision, Free Motion Laparoscopic Surgical System," ASME Paper No. DMD2022-1021.

[23] Tahan, N., Khademi-Kalantari, K., Mohseni-Bandpei, M. A., Mikaili, S., Baghban, A. A., and Jaberzadeh, S., 2016, "Measurement of Superficial and

Deep Abdominal Muscle Thickness: An Ultrasonography Study," J. Physiol. Anthropol., **35**(1), p. 17.
[24] Störchle, P., Müller, W., Sengeis, M., Lackner, S., Holasek, S., and Fürhapter-Rieger, A., 2018, "Measurement of Mean Subcutaneous Fat Thickness: Eight Standardised Ultrasound Sites Compared to 216 Randomly Selected Sites," Sci. Rep., **8**(1), p. 16268.
[25] Jain, S. M., Pandey, K., Lahoti, A., and Rao, P. K., 2013, "Evaluation of Skin and Subcutaneous Tissue Thickness at Insulin Injection Sites in Indian, Insulin Naïve, Type-2 Diabetic Adult Population," Indian J. Endocrinol. Metab., **17**(5), pp. 864–870.
[26] Hu, Z., Sun, W., and Zhang, B., 2013, "Characterization of Aortic Tissue Cutting Process: Experimental Investigation Using Porcine Ascending Aorta," J. Mech. Behav. Biomed. Mater., **18**, pp. 81–89.
[27] de Beaufort, H. W. L., Ferrara, A., Conti, M., Moll, F. L., van Herwaarden, J. A., Figueroa, C. A., Bismuth, J., Auricchio, F., and Trimarchi, S., 2018, "Comparative Analysis of Porcine and Human Thoracic Aortic Stiffness," Eur. J. Vasc. Endovasc. Surg., **55**(4), pp. 560–566.
[28] Sykes, M., and Sachs, D. H., 2019, "Transplanting Organs From Pigs to Humans," Sci. Immunol., **4**(41), p. eaau6298.